Improved temporal contrast of streak camera measurements with periodic shadowing

Bao, Yupan; Kornienko, Vassily; Lange, David; Kiefer, Wolfgang; Eschrich, Tina; Jäger, Matthias; Bood, Joakim; Kristensson, Elias; Ehn, Andreas

Published in:
Optics Letters

DOI:
10.1364/OL.438034

2021

Document Version:
Publisher's PDF, also known as Version of record

Optics Letters

Improved temporal contrast of streak camera measurements with periodic shadowing

Yupan Bao,[1] Vassily Kornienko,[1] David Lange,[1] Wolfgang Kiefer,[2,3] Tina Eschrich,[4] Matthias Jäger,[4] Joakim Bood,[1] Elias Kristensson,[1] and Andreas Ehn[1,*]

[1]Department of Combustion Physics, Lund University, P.O. Box 118, S-221 00 Lund, Sweden
[2]Institute for Physical and Theoretical Chemistry, University of Würzburg, 97074 Würzburg, Germany
[3]Eisingen Laboratory for Applied Raman Spectroscopy, 97249 Eisingen, Germany
[4]Leibniz Institute of Photonic Technology, Albert Einstein St. 9, 07745 Jena, Germany
*Corresponding author: andreas.ehn@forbrf.lth.se

Received 13 August 2021; revised 23 September 2021; accepted 25 September 2021; posted 28 September 2021; published 15 November 2021

Periodic shadowing, a concept used in spectroscopy for stray light reduction, has been implemented to improve the temporal contrast of streak camera imaging. The capabilities of this technique are first proven by imaging elastically scattered picosecond laser pulses and are further applied to fluorescence lifetime imaging, where more accurate descriptions of fluorescence decay curves were observed. This all-optical approach can be adapted to various streak camera imaging systems, resulting in a robust technique to minimize space-charge induced temporal dispersion in streak cameras while maintaining temporal coverage and spatial information.

https://doi.org/10.1364/OL.438034

Streak cameras [1–3] were invented by Courtney-Pratt in 1949 [4,5] in order to capture fast transient phenomena, which are beyond the temporal resolution of traditional mechano-optical cameras. Their ability to simultaneously provide spatial and temporal information at sub-picosecond (even up to attosecond [6,7]) resolution was first used to characterize ultrashort laser pulses generated by mode-locked laser systems [8]. Over the years, the streak camera has become a robust workhorse for capturing rapid dynamics of luminous phenomena within the fields of biology, chemistry, physics, and medicine, with applications ranging from fluorescence lifetime imaging [9,10] to ultrafast electron microscopy [1,2,11].

The working principle of a streak camera is illustrated in Fig. 1(a) [12]. The signal of interest is first imaged onto a slit where the one-dimensional (1D) spatial information is retained. Signal photons are converted into photoelectrons via a photocathode. These will be accelerated through a mesh before entering the sweeping tube, where a voltage ramp is applied, giving the electrons a tangential velocity perpendicular to the direction of propagation. The signal electrons, which reach the sweeping tube at different times, experience different electric fields. Consequently, they will arrive at the detector at different positions, resulting in a time-dependent spatial distribution of the signal. The resulting image, hence, retains the slit's spatial information in one dimension and the signal's temporal information in the second dimension.

A side effect of the voltage ramp inside the sweeping tube is that any initial velocity distribution of electrons entering the tube translates directly into a temporal dispersion in the final image output. Hence, a wider velocity distribution, caused by, e.g., the space-charge effect at the photocathode [14], directly translates into a broader temporal profile (pulse broadening), degrading the temporal resolution of the streak camera. Various solutions have been proposed and implemented to minimize this effect. Some examples include: inserting a reflectron to compensate for the energy spread of the initial photoelectrons by giving them a higher energy and longer flight path [15,16]; shortening the distance between the photocathode and mesh to reduce space-charge related electron pulse broadening in said region [2,3,17]; implementing specially designed photocathodes, lens systems, and streaking tubes with optimized working voltage [18,19]; and adding a two-dimensional (2D) to 1D fiber array with certain time delays between adjacent fibers to reduce the cross talk between the input channels [20,21].

In this Letter, we propose an all-optical approach to further reduce the temporal dispersion of streak camera imaging in the form of periodic shadowing (PS) [12]. Due to the low experimental complexity of this approach, it can be readily adapted to any streak camera imaging system, regardless of the sweeping method or implemented opto-electronic improvement while maintaining both temporal coverage and spatial information.

PS of the signal is here implemented in two configurations: either with a Ronchi grating [12] or an optical fiber bundle [13]. An example of a single-shot streak camera signal of two consecutive scattered laser pulses coded with PS is shown in Fig. 1(c). Its Fourier transform [Fig. 1(d)] displays separated Fourier components of the tagged signal, where the signal of interest is marked by an ellipse. The tagged signal can be extracted by first shifting its Fourier components to the origin and subsequently applying

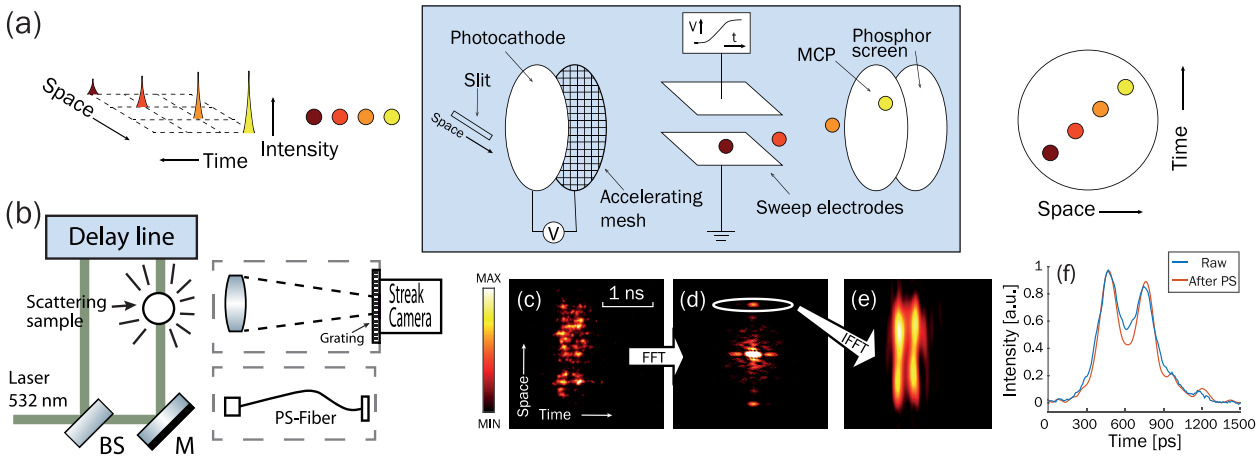

Fig. 1. (a) Simplified sketch of a streak camera. (b) A sketch of the experimental setup: BS, beam splitter; M, mirror; streak camera, OptoScope S20 with FTSI1-ST, operated in single-shot mode; laser, Ekspla SL334; grating, Ronchi Grating (5, 7, 4.8 lp/mm); PS-fiber, equivalent to the one found in [13]. The grating and PS fiber-based setups are interchangeable, without affecting the rest of the setup. (c) An example of a single-shot streak camera signal of two successive scattered laser pulses, using periodic shadowing (PS). (d) The Fourier transform of (c) where the modulated signal is encircled by the ellipse. (e) Inverse Fourier transform of the first order component filtered out by the Gaussian ellipse filter from (d). (f) Comparison of the normalized intensity of the laser pulses obtained before and after postprocessing in the Fourier domain.

a Gaussian filter. The inverse Fourier transform of the recentered and filtered image results are shown in Fig. 1(e). More technique details of PS can be found in Supplement 1. A drawback of PS is the sacrifice of spatial resolution due to the application of a low-pass filter. Hence, for streak camera applications, where the temporal resolution is of importance, an elliptical low-pass filter is chosen. Its large semi-major axis retains the temporal resolution of the streak camera while the small semi-minor axis effectively isolates the PS signal from the DC background. A comparison of the normalized intensity of the signal processed with/without PS shows clear signal reduction in the region between the two pulses [Fig. 1(f)]. Furthermore, an inherent advantage of PS is the automatic subtraction of the DC component. This is advantageous especially when the background is nonlinear to the signal, where conventional methods to record the background, e.g., a black recording without any signal, become impractical.

The improvement of temporal contrast when using PS on streak camera measurements is demonstrated by (1) imaging a single and two consecutive laser pulses incident on a scattering medium and (2) measuring the temperature-dependent fluorescence lifetime of a Rhodamine 610 solution.

The results of applying PS (7 lp/mm) to the imaging of a scattered laser pulse at a streak rate of 7 ps/px, correcting for streak camera jitter, and averaging over 100 shots are shown in Fig. 2(a). Here, the effect of PS is to eliminate artefacts that arise in the beginning and end of the peak (the total integrated area is 85.4% that of the non-PS peak), effectively reducing the FWHM from 320 to 280 ps. The inset in Fig. 2(a) illustrates the automatic baseline correction obtained from PS due to the elimination of DC background after applying the low-pass filter. The trend of lower FWHM for the PS signal continues for all streak rates until it converges with the non-PS signal at 1.4 ps/px [Fig. 2(b)]. At this streak rate, the camera has sufficient temporal resolution for single pulse measurements such that the pulse broadening caused by space-charge effects is negligible compared to the pulse length. However, in combination with

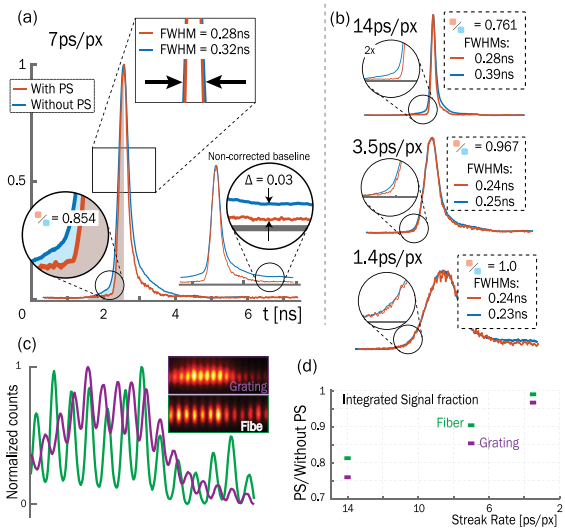

Fig. 2. Results of applying PS to the imaging of a single scattered laser pulse at (a) a streak rate of 7 ps/px and (b) higher streak rates. (c) Comparision of the modulation depth of the signal between the use of grating and fiber bundle. (d) Integration of the signal with divided by without PS at different streak rates. All data were averaged over 100 shots with jitter correction.

PS, the same temporal resolution could be achieved at lower streak rates, where higher temporal coverage and higher SNR are attained.

The measurements were also repeated with an optical fiber bundle, where the lower acceptance angle of the fiber, in conjunction with more efficient light shielding as compared to an imaging system based on a Ronchi grating, further eliminates background scattered light from entering the streak camera. This has the effect of increasing the modulation depth of the PS pattern [Fig. 2(c)], allowing for a larger share of dynamic range allocated to the modulated signal. Figure 2(d) compares the integration fraction (PS/without PS) for the grating (in this

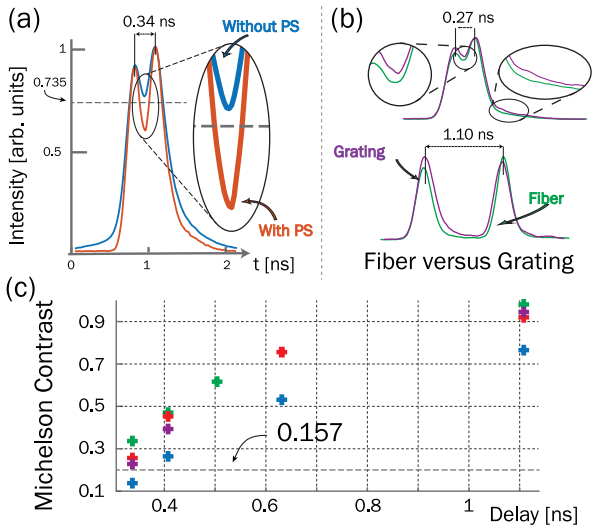

Fig. 3. (a) Two scattered Gaussian laser pulses are brought from a temporally unresolved to resolved regime using PS (with the streak of 7 ps/px). (b) Performing the same investigation with a fiber bundle further increases the temporal resolution due to the larger modulation depth. (c) Michelson contrast of the raw data (blue), grating of 5 lp/mm (red) and 7 lp/mm (purple), and fiber bundle or 4.8 lp/mm (green).

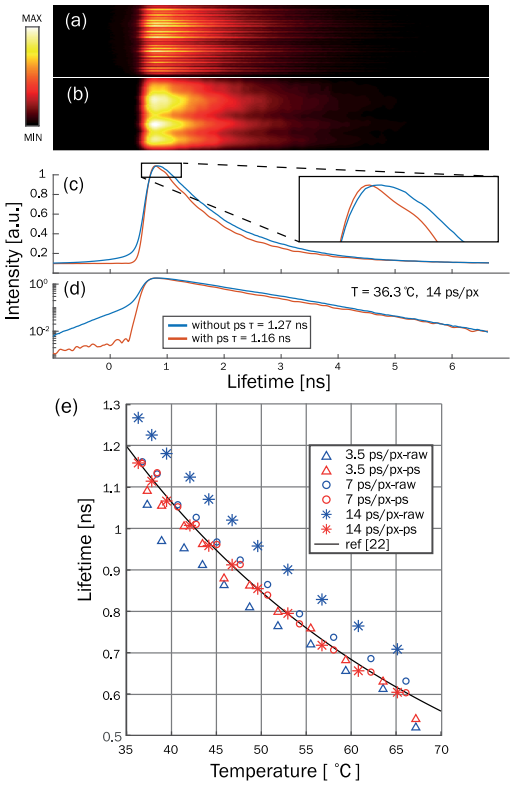

Fig. 4. Fluorescence lifetime measurements of Rhodamine 610. (a) The raw image. (b) The postprocessed image using PS. (c), (d) Intensity curves derived from the raw image (blue) and the processed image (magenta) in linear scale (c) and logarithmic scale (d). (e) Temperature-dependent lifetime calculated from the measured curve with different streak rates. The reference curve originates in the Arrhenius equation, $\frac{1}{\tau} = A \exp(\frac{-E_a}{RT})$ with E_a the apparent activation energy, equal to 19.2 kJ/mol.

case 5 lp/mm, indicated in purple) and fiber bundle (4.8 lp/mm indicated in green) as a function of streak rate. An integration fraction below unity, even for measurements that have reduced amounts of background light, (i.e., measurements with the fiber bundle), substantiates that PS not only eliminates background stray light that enters the camera but is also efficient at reducing the temporal dispersion caused by space-charge effects within the streak camera.

To further validate PS, the PS with streak camera combination was implemented in order to characterize a two-pulse picosecond pulse train. Inspired by the Rayleigh criteria for spatially resolved point sources, two Gaussian pulses are said to be temporally resolved herein if their summed intensity falls below a Michelson contrast of 0.735 (see Supplement 1). As a result of the increased temporal contrast attainable with PS, two consecutive scattered Gaussian laser pulses were brought from a temporally unresolved to resolved regime [Fig. 3(a)]. Although not as critical, this trend continues for increased inter-pulse delay times, for which a higher Michelson contrast is maintained [Fig. 3(c)]. Moreover, performing PS with a fiber bundle has the effect of even further increasing the contrast between two pulses [Figs. 3(b) and 3(c)].

Temperature-dependent fluorescence lifetime measurements of a Rhodamine 610 and water solution (3×10^{-9} M) were carried out with a 5 lp/mm Ronchi grating and streak rates of 14 ps/px, 7 ps/px, and 3.5 ps/px. A streak rate of 1.4 ps/px could not be applied to these measurements as the whole decay would not fit on the sensor. Furthermore, the temporal jitter is too large at this streak rate (in relation to the temporal coverage) to allow for efficient jitter correction. This fact exemplifies the need for PS, as it can increase the temporal resolution (in the same way that increasing streak rate does) while maintaining temporal coverage and the possibility to perform jitter correction. An example is given in Figs. 4(a)–4(d), where a significant amount of background has been eliminated with PS, especially in the rising edge. Although not as obvious, the interfering background on the falling edge has also been filtered out, increasing the accuracy of the decay curve for this Rhodamine sample. Accuracy in this part of the signal is critical for lifetime measurements, as a slight difference in its shape can cause a significant change in the calculated lifetime. For example, the difference in lifetime calculated from the curve processed with and without PS is around 100 ps (at a streak rate of 14 ps/px). This corresponds to more than 15% of the actual lifetime, about 600 ps, of Rhodamine 610 at 65°C. The calculated lifetimes from both the PS-corrected and original curves are plotted in Fig. 4(e) with reference data (from [22]). Good agreement between [22] and the PS measurements is observed. Detailed data of the decay curves of fluorescence lifetime measurements and parameter study of the size of the ellipse filter applied using PS can be found in Supplement 1.

In contrast to Fig. 2(b), where PS has a smaller effect for the calculation of FWHM at higher streak rates, in the context of lifetime measurements, the increased accuracy of lifetime evaluation is significant even for streak rates of 3.5 ps/px. This should be credited to the efficient removal of background interference in the form of stray light and space-charge effect, which in itself is a sensitive parameter for accurate lifetime determination. Moreover, unlike the measurements with streak rates of 14 and 7 ps/px, the lifetime calculated from the processed curve

is not only more accurate but also longer with a streak rate of 3.5 ps/px. This shows that PS not only deals with stray light, whose removal via the subtraction of a black field image always leads to a shorter lifetime, but also background interference introduced by the aforementioned space-charge effect.

The underlying principle of a streak camera is its ability to convert temporal into spatial information. This allows for its temporal resolution to be independent of exposure time, frame-rate, and pixel readout speed (as is the case with conventional cameras) setting its minimum temporal dispersion to the streak rate in seconds per pixel. However, the complex photon-electron conversion steps involved result in an actual temporal dispersion that is instead limited by, e.g., space-charge effects on the streak unit, blooming in the multi-channel plate, and imperfections in the imaging system.

The optical configuration of PS has several technical advantages over traditional, electronic-based streak camera improvements. First, applying a grating to the imaging configuration of the setup is a versatile approach that can be readily used and tailored to fit to a specific streak camera measurement configuration. Second, even though the camera can attain streak rates that are high enough to temporally resolve all laser pulse measurements presented herein, it does so at the cost of temporal coverage and decreased signal per pixel (resulting in decreased SNR). PS compensates for this by allowing for higher temporal resolution at a given streak rate, hence maintaining the higher signal per pixel available at lower streak rates. Third, the use of a fiber bundle, in itself resulting in an increased modulation depth and final temporal contrast as compared to a grating, grants this technique (in its fiber-based configuration) access to difficult *in situ* measurement configurations, such as a pressure/vacuum chamber with limited optical access. Finally, the significant decrease of pulse broadening, along with the elimination of the DC component, allows for accurate streak camera-based optical lifetime measurements, introducing an alternative to conventional lifetime measurement configurations.

The increased necessity of high-speed optical measurement techniques across the sciences has brought the streak camera into a diverse set of labs. However, at these breakneck speeds, its temporal resolution is usually limited by pulse broadening effects within the electronics. Even though there exist solutions, these are always targeted at the opto-electronic components, which have already been pushed to their extremes. The work presented herein offers a versatile, all-optical approach to simultaneously increasing the temporal resolution of a streak camera while maintaining temporal coverage and spatial information, adapting streak cameras to applications within a wider range of fast transient events.

Funding. European Research Council (669466, 803634, 852394); Vetenskapsrådet (2019-05183, 2015-05321); Knut och Alice Wallenbergs Stiftelse (2019.0084); Energimyndigheten (22538-4).

Disclosures. The authors declare no conflicts of interest.

Data Availability. Some of the data underlying the results presented in this Letter are available in Supplement 1. The other data can be obtained from the authors upon reasonable request.

Supplemental document. See Supplement 1 for supporting content.

REFERENCES

1. A. Campillo and S. Shapiro, IEEE J. Quantum Electron. **19**, 585 (1983).
2. C. Johnson, *High Speed Optical Techniques: Developments and Applications* (SPIE, 1977), Vol. **94**, pp. 13–18.
3. A. Huston, J. Phys. E **11**, 601 (1978).
4. J. Courtney-Pratt, Research **2**, 287 (1949).
5. J. Courtney-Pratt, Proc. R. Soc. London A **204**, 27 (1950).
6. J. Itatani, F. Quéré, G. L. Yudin, M. Y. Ivanov, F. Krausz, and P. B. Corkum, Phys. Rev. Lett. **88**, 173903 (2002).
7. M. Ivanov and O. Smirnova, Phys. Rev. Lett. **107**, 213605 (2011).
8. D. Bradley and G. H. New, Proc. IEEE **62**, 313 (1974).
9. K. Suhling, L. M. Hirvonen, J. A. Levitt, P.-H. Chung, C. Tregidgo, A. Le Marois, D. A. Rusakov, K. Zheng, S. Ameer-Beg, S. Poland, S. Coelho, R. Henderson, and N. Krstajic, Med. Photon. **27**, 3 (2015).
10. J. Qu, L. Liu, D. Chen, Z. Lin, G. Xu, B. Guo, and H. Niu, Opt. Lett. **31**, 368 (2006).
11. W. E. King, G. H. Campbell, A. Frank, B. Reed, J. F. Schmerge, B. J. Siwick, B. C. Stuart, and P. M. Weber, J. Appl. Phys. **97**, 111101 (2005).
12. E. Kristensson, J. Bood, M. Alden, E. Nordström, J. Zhu, S. Huldt, P.-E. Bengtsson, H. Nilsson, E. Berrocal, and A. Ehn, Opt. Express **22**, 7711 (2014).
13. M. Gong, H. Kim, J. Larsson, T. Methling, M. Aldén, E. Kristensson, C. Brackmann, T. Eschrich, M. Jäger, W. Kiefer, and A. Ehn, Opt. Express **29**, 7232 (2021).
14. Z. Tao, H. Zhang, P. M. Duxbury, M. Berz, and C.-Y. Ruan, J. Appl. Phys. **111**, 044316 (2012).
15. U. Boesl, R. Weinkauf, and E. W. Schlag, Int. J. Mass Spectrom. Ion Processes **112**, 121 (1992).
16. Y. Wang and N. Gedik, IEEE J. Sel. Top. Quantum Electron. **18**, 140 (2012).
17. B.-L. Qian and H. E. Elsayed-Ali, J. Appl. Phys. **91**, 462 (2001).
18. H. Niu, H. Zhang, Q. L. Yang, Y. P. Liu, Y. C. Wang, Y. A. Reng, and J. L. Zhou, Proc. SPIE **1032**, 472 (1989).
19. H. Niu, V. P. Degtyareva, V. N. Platonov, A. M. Prokhorov, and M. Y. Schelev, Proc. SPIE **1032**, 79 (1989).
20. N. Hirmiz, A. Tsikouras, E. J. Osterlund, M. Richards, D. W. Andrews, and Q. Fang, Opt. Express **27**, 22602 (2019).
21. A. Tsikouras, J. Ning, S. Ng, R. Berman, D. W. Andrews, and Q. Fang, Opt. Lett. **37**, 250 (2012).
22. R. Mercade-Prieto, L. Rodriguez-Rivera, and X. D. Chen, Photochem. Photobiol. Sci. **16**, 1727 (2017).